Clays and Clay Minerals, Vol. 58, No. 5, 691–706, 2010.

SEASONAL VARIATION IN THE MINERALOGY OF THE SUSPENDED PARTICULATE MATTER OF THE LOWER CHANGJIANG RIVER AT NANJING, CHINA

CHANGPING MAO[1,*], JUN CHEN[1], XUYIN YUAN[2], ZHONGFANG YANG[3], WILLIAM BALSAM[4,†], AND JUNFENG JI[1]

[1] Institute of Surficial Geochemistry, Department of Earth Sciences, Nanjing University, Nanjing 210093, China
[2] College of Environmental Science and Engineering, Hohai University, Nanjing 210098 , China
[3] School of Earth Science and Resources, China University of Geosciences (Beijing), Beijing 100083, China
[4] Department of Earth and Environmental Sciences, University of Texas at Arlington, Arlington, TX 76019, USA

Abstract—The source and temporal changes of minerals transported by the world's large rivers are important. In particular, clay minerals are important in evaluating the maturity of suspended sediments, weathering intensity, and source area. To examine seasonal changes in mineralogical compositions of the Changjiang River (CR), suspended particulate matter (SPM) samples were collected monthly for two hydrological cycles in Nanjing city and then were studied using X-ray diffraction (XRD), diffuse reflectance spectrophotometry (DRS), X-ray fluorescence spectrometry (XRF), and chemical analyses. The results indicate that the concentration of CR SPM ranges from 11.3 to 152 mg/L and is highly correlated to the rate of water discharge, with a greater concentration in flood season and lower concentrations during the dry season. CaO, MgO, and Na_2O increase with increasing discharge whereas Al_2O_3 decreases sharply with increasing discharge. Dolomite, calcite, and plagioclase show strikingly similar seasonal variations and increase with increasing discharge with maximum concentrations in the flood season. In contrast, the clay mineral content exhibits the opposite trend with the lowest concentrations in the flood season. Illite dominates the clay minerals of the CR SPM, followed by chlorite, kaolinite, and smectite. Illite and kaolinite show distinctly seasonal variations; SPM contains more illite and less kaolinite during the flood season than during the dry season. The illite chemistry index and crystallinity, as well as kaolinite/illite ratio, all indicate intense physical erosion in the CR basin during the rainy season. Total iron (Fe_T) and highly reactive iron (Fe_{HR}) concentrations display slight seasonal changes with the smallest values observed during the flood season. Goethite is the dominant Fe oxide mineral phase in the CR SPM and hematite is a minor component, as revealed by DRS analyses. The Fe_T flux and Fe_{HR} flux are 2.78×10^6 T/y and 1.19×10^6 T/y, respectively.

Key Words—Changjiang River, Erosion, Mineralogy, Seasonality, Suspended Particulate Matter.

INTRODUCTION

Continental erosion is a major geological process which is influenced by meteoric water and many other factors including glaciers, wind, and vegetation. Rainwater and surface water interact with minerals on the Earth's surface, resulting in the dissolution of primary minerals and the production of secondary clays and (oxyhydr)oxides of Fe and Al. The weathering of continental rocks and the subsequent transport of weathering products by rivers accounts for most of the solutes and particulate materials delivered to oceans (Martin and Meybeck, 1979; Milliman and Meade, 1983).

The Changjiang River (Yangtze River) is the world's third longest river (6300 km) and it's fourth largest in terms of water discharge (Chen *et al.*, 2002) (Figure 1). It is characterized by high elevation in the inner part of the catchment basin, a monsoon climate, and intense weathering in lower parts of the basin, resulting in large freshwater and sediment discharges. The Changjiang River, therefore, is one of the most important SPM-transporting rivers in the world. The modern Yangtze River's annual sediment load is ~480 million tons (Milliman and Meade, 1983). The CR has long been considered the dominant contributor to the inner-shelf mud wedge in the East China Sea (Xu *et al.*, 2009). The dissolved and particulate fluxes carried by CR are an important link in biogeochemical cycling between land and ocean. As a result, numerous studies have addressed the geochemistry of suspended and dissolved material in the river (Hu *et al.*, 1982; Li *et al.*, 1984; Zhang, 1999; Zhang *et al.*, 1998; Zhang *et al.*, 1990; Chen *et al.*, 2002; Ding *et al.*, 2004; Wang *et al.*, 2007; Koshikawa *et al.*, 2007; Chetelat *et al.*, 2008; Muller *et al.*, 2008; Gao and Wang, 2008).

A large part of the CR Basin has a subtropical monsoon climate. As water discharge is subject to strong seasonality, the suspended particulate matter of the CR varies considerably according to the season and from one year to another. Most sediment transportation takes

* E-mail address of corresponding author:
chpmao@nju.edu.cn
†Current address: 209 Camino de Santiago, Taos, New Mexico 87571, USA
DOI: 10.1346/CCMN.2010.0580508

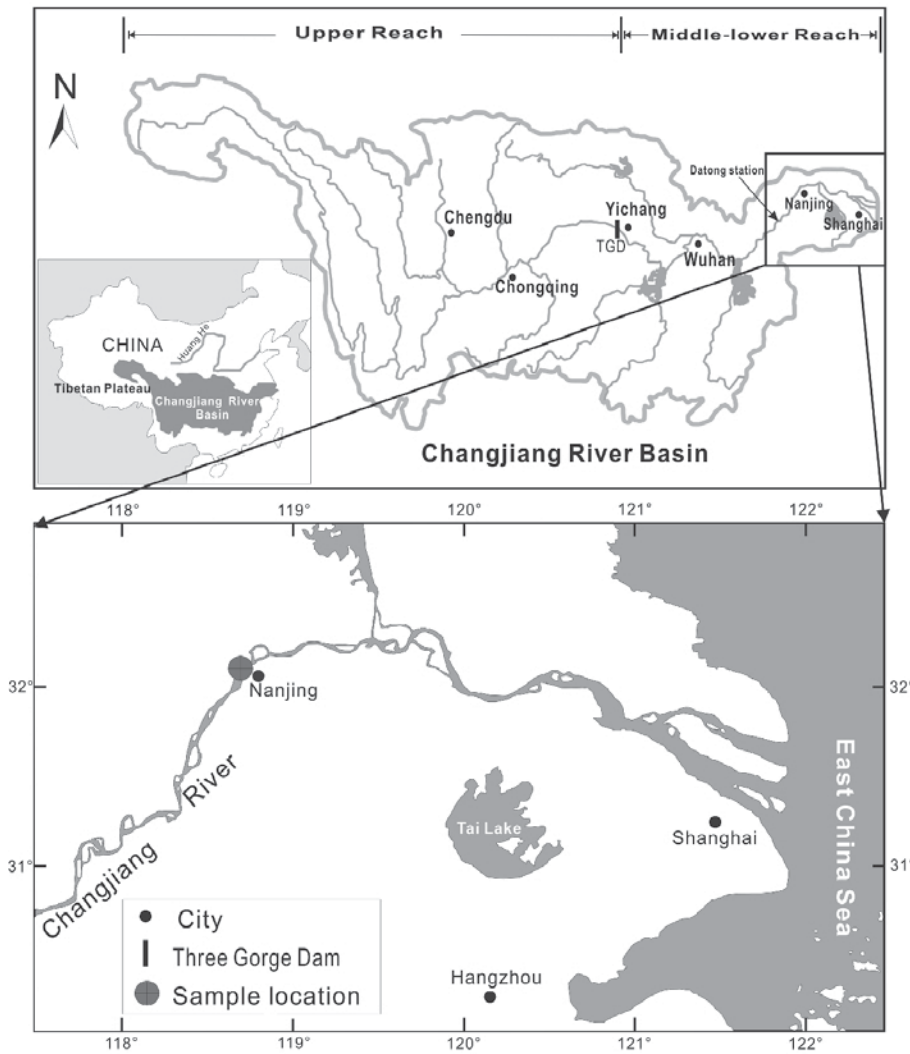

Figure 1. Map of the Changjiang River drainage basin and sampling site.

place in the summer half of the year, from May to October. Several studies have investigated seasonal variations in the geochemistry of dissolved and particulate matter, *e.g.* Zhang (1999) found differences in metal concentration of the suspended particulate matter between dry and flood seasons. Chen *et al.* (2002) studied the chemical composition of the river water throughout the basin based on monthly monitored chemical data at 191 stations for the period from 1958–1990. Duan *et al.* (2008) reported the seasonal changes in the transport of nitrogen and phosphorus (from June 1998 to March 1999) from the CR to the East China Sea. Seasonal mineral changes of the SPM have not previously been investigated in detail, however.

In most cases, minerals are the major contributors to suspended particulate matter which is transported by rivers to the ocean. Suspended mineral phases in rivers are sensitive to environmental changes caused by natural processes and human activities and may, therefore, be useful indicators of events which last long enough to exhibit their effects on the environment (Dekov *et al.*, 1997; Viers *et al.*, 2009). Knowledge of changes in the mineralogy in a major river system may help to advance understanding of variations in continental material supplied to the oceans and weathering rates related to climate (Eberl, 2004). Evidence for environmental and climatic conditions is often preserved in the clay fraction of sediments and soils.

The physical and chemical properties of clay minerals are good indicators of sediment sources and the composition and climate in the source area, and their distribution patterns in sedimentary basins may be indicative of the main transport processes and pathways (Chamley, 1989; Weaver, 1989; Balsam and Beeson,

2003; Guyot *et al.*, 2007). Clay mineral assemblages have also been used successfully to trace oceanic current patterns (Petschick *et al.*, 1996; Gingele *et al.*, 2001). In addition, the distribution of recent clay mineral assemblages in the world's ocean in combination with down-core records have been used as paleoclimatic and paleo-oceanographic indicators (Thiry, 2000; Liu *et al.*, 2003).

In sediments and soils under the Earth's surface conditions, iron (Fe) occurs predominantly as Fe^{3+} in the form of sparingly soluble Fe-(oxyhydr)oxide minerals such as ferrihydrite, goethite, and hematite (Cornell and Schwertmann, 2003). The Fe supply reaches the oceans mainly from rivers as suspended sediment in a vast global transport system (Poulton and Raiswell 2002; Jickells *et al.*, 2005). Solid-phase Fe^{3+} plays an important role in marine depositional environments and the Fe cycle (Haese, 2006). Furthermore, Fe can affect primary productivity in major ocean regions (Fung *et al.*, 2000; Jickells *et al.*, 2005) only if it exists in a readily soluble form. Poulton and Raiswell (2005) showed that a significant proportion of the (oxyhydr)oxide Fe in riverine suspended sediment exists as nanoparticles that are potentially bioavailable. In addition, Fe (oxyhydr)oxides may play an important role in the retardation of the transport of different contaminants and the bio-availability of nutrients because they are present in many natural media in contact with water, and they have well known high sorption and co-precipitation capacities for a number of trace elements (Rovira *et al.*, 2008; Cornell and Schwertmann, 2003) and nutrients, *e.g.* phosphorus (Paige *et al.*, 1997; Borch *et al.*, 2007; Gimsing and Borggaard, 2007).

The goal of the present work was to examine in detail the temporal distribution of mineral species in the CR SPM through seasonal sampling and examine factors that control their seasonal variations. Information from this work will also contribute to the understanding of sediment transport by the CR and variation in mineralogy found off the river mouth. Special emphasis will be placed on investigating Fe speciation and the flux of Fe species to the ocean for a one-year hydrological cycle.

NATURAL SETTING OF THE CHANGJIANG RIVER

Geographical and geological background

The CR originates on the Tibetan Plateau at 5100 m elevation and enters the East China Sea (Figure 1) with a water discharge of ~8.94×10^{11} m^3/y (Chen *et al.*, 2001). Its drainage basin is situated between 25ºN and 35ºN and 90ºE and 122ºE, and covers a total area of 181×10^4 km^2, nearly 20% of the total terrestrial area of China. The river is generally divided into two parts: the upper CR and the mid−lower CR. The upper reaches are 4500 km long, from the source region to Yichang, and the mid−lower reaches are 1800 km long, from Yichang to the East China Sea. The geomorphology is characterized by mountains and hills in the upstream areas and by extensive fluvial plains with numerous lakes in the downstream areas. About half of the river water and most of the SPM are derived from the upper CR basin (Chen *et al.*, 2001; Yang *et al.*, 2002). In its mid−lower part, the CR drains one of the most populated areas of the world and is affected by the Three Gorges Dam (TGD), the biggest dam in the world (Figure 1).

The majority of the CR basin lies in the Yangtze Craton framed by the Mesozoic Yanshanian orogenic belt (Yang *et al.*, 2004). The complicated source-rock types in the drainage basin comprise Archean metamorphic rocks and Mesozoic−Cenozoic igneous and sedimentary rocks, including clastics, marine carbonates, evaporites, and alluvium from Precambrian to Quaternary in age. The CR basin can be divided into two regions: (1) The upper basin is characterized by complex rock compositions, including clastic sedimentary rocks, igneous rocks, and metamorphic rocks throughout the Qinghai-Tibet Plateau to the city of Yibin (Ding *et al.*, 2004). Jurassic red sandstone is distributed widely in the Sichuan Basin. Evaporites are found mainly in the upper reaches of the CR (Chen *et al.*, 2002). Carbonate rocks are widespread over the basin and are particularly abundant in the southern parts of the upper reaches (Yunnan, Guizhou and western Hunan Provinces). (2) The middle−lower basin mostly consists of Paleozoic marine and Quaternary fluvio-lacustrine sedimentary rocks together with intermediate to felsic igneous rocks that are common, but sporadic (Yang *et al.*, 2004). Along the river, mainly Quaternary fluvial and lacustrine sediments crop out, and large areas of wetlands and paddy fields (Ding *et al.*, 2004) are common, not only along the main channel of the CR, but also its tributaries and the nearby lakes.

Hydrological mean features

Except for the source area for the CR (headwater) characterized by high elevation and cold climate, most of the CR Basin is located in the subtropical zone influenced by a typical East Asian monsoon climate that is temperate and humid. The annual mean temperature is <4ºC in the source area, 5−15ºC in the upper reaches which are mountainous areas, and 16−18ºC in the middle and lower reaches. The long-term mean of the annual precipitation in the CR basin is ~1070 mm, but the spatial and temporal precipitation distribution is highly irregular. Annual precipitation decreases gradually from southeast to northwest, from 1644 mm/y for the lower reach, 1396 mm/y for the middle reach, and 435 mm/y for the upper reach (Chen *et al.*, 2001). Surface runoff is the major water supply for the Changjiang watershed, accounting for 70−80% of the total water discharge (Chen *et al.*, 2002). The geomorphology is characterized by mountains and hills in the

upstream areas and extensive fluvial plains with numerous lakes in the downstream areas. The CR sediment mainly comes from the NW of the CR basin because of the presence of more erodible soils and steep mountains. The upper CR basin also supplies most of the suspended sediments to the ocean (Yang *et al.*, 2002; Xu *et al.*, 2007; Chen *et al.*, 2008). The sediment supply from middle–lower reaches of the river basin is much smaller in quantity in comparison with that from the upstream (Chen *et al.*, 2008).

Under the control of the Asian summer monsoon, water and sediment discharge from both the Yangtze's upper and lower reaches show seasonal patterns (Xu and Milliman, 2009). The precipitation and runoff change seasonally with 70–80% in the rainy season (summer) from May to October (Yang *et al.*, 2002). From 1950–1990, >70% of water discharge of the CR occurred during summer (May–October), with an average peak in July (Xu and Milliman, 2009). The modern Yangtze River discharges most of its annual sediment load between June and September (Liu *et al.*, 2007).

The Yangtze River transported ~900 billion m^3 of water into the sea each year and carried ~434×10^6 tons of sediment before the completion of the TGD project (Chen *et al.*, 2008). Although the dams had little impact on water discharge, the sediment load has declined dramatically in response to the presence of the dams (Xu *et al.*, 2006). The TGD began to impound water and sediment on 1 June 2003 (Xu and Milliman, 2009). For 2006, the sediment discharge recorded at Datong (a gauging station in the lower reach) fell to 85×10^6 tons compared to the 434×10^6 tons observed during the period 1953–2000 (Chen *et al.*, 2008). Although sediment discharge has decreased sharply because of dam construction, the upper CR basin supplied most of the suspended sediments to the ocean (Chen *et al.*, 2008) and the TGD impoundment had little impact on the seasonal sediment discharge pattern (large sediment discharge in flood season and low sediment discharge in dry season) in the lower reaches (Xu and Milliman, 2009).

MATERIALS AND METHODS

Sampling and analysis

Seasonal variations were examined by taking monthly SPM samples from the lower CR stream at Nanjing city (Figure 1) for 2 y. The study reported here focuses on the second of the two years. The first year included only two samples, one from 5 January 2005 (dry season) and the other from 18 August 2005 (flood season). All samples were taken at the same location, N32º05′33.9″, E118º43′27.6″. During the second year, samples of SPM were collected monthly from 28 October 2006 to 24 September 2007.

Water-sample collection was carried out from a boat in the middle of the river channel at a water depth of ~30 cm. Samples were collected in acid-cleaned containers and filtered through 0.45 μm Millipore membranes (defined here as the size fraction ranging from 63 to 0.45 μm).

In addition, two samples were collected at Chongqing city (E107º17′30.3″, N29º43′42.4″) in the upper reaches of CR (in the upstream of the TDG) during 7 September 2007 (flood season) and 29 December 2007 (dry season) (Figure 1). These two samples (Chongqing) were used for clay-mineral analysis.

Pretreatment for grain-size analysis included removal of organic matter using hydrogen peroxide (H_2O_2) and the addition of sodium hexametaphosphate $(NaPO_3)_6$ to further disperse the sediment. The grain-size distribution of the SPM was measured with a Malvern Mastersizer S Laser instrument at the Institute of Earth Environment, Chinese Academy of Sciences.

Major elements were analyzed by X-ray fluorescence using an ARL9800XP$^+$ X-ray fluorescence spectrometer (XRF) at the Center of Modern Analyses, Nanjing University. The 0.6 g sample was mixed with 6.6 g of the fluxing agent Li tetraborate and Li metaborate ($Li_2B_4O_7/LiBO_2$ = 67/33), and then the mixed sample was added to a 120 mg/L LiBr flux in a platinum crucible. The mixture was then fused using an automatic gas-fired CLAISSE burner system to make a glass disc for XRF measurement.

Identification and quantification of minerals

The mineralogy of the bulk samples was determined by X-ray diffraction (XRD). Semi-quantitative estimates of mineral concentration were obtained by applying the correction factors determined by Cook *et al.* (1975) and Boski *et al.* (1998) to the measured intensities of reflections.

The clay fraction was separated from the bulk samples based on Stokes' Law, suspended in deionized water, and allowed to dry on glass slides to form oriented aggregates. Before XRD analysis the clay fraction was air dried, solvated for 12 h over a bowl of ethylene glycol (EG) in an oven at 60ºC, and heated to 550ºC for 2 h. Selected samples of the clay fraction also were treated with HCl (3 mol/L) for 2 h at 80ºC to remove acid-labile silicates. Semi-quantitative estimates of relative clay-mineral percentages were obtained from measurement of XRD pattern peak areas, which were multiplied by the weighting factors of Biscaye (1965): four times the illite peak area, two times the kaolinite + chlorite peak area, and one time the smectite peak area, then normalized to 100%. The relative proportion of kaolinite and chlorite was determined on the basis of the ratio of the 3.57/3.54 Å peak areas.

Clay minerals were identified according to the position of the (001) series of basal reflections on the XRD patterns of air-dried, ethylene glycolated, HCl- and heated-treated specimens (Figure 8). Illite was identified by the basal 10 Å peak; this basal spacing remains

unaffected after glycolation, heating, and HCl treatment. Kaolinite was recognized by its 7 Å peak which disappears after heating to 550ºC but does not disappear after HCl treatment (chlorite is dissolved and kaolinite remains). Smectite exhibits a broad 12−15 Å reflection which increases to 17 Å after saturation with ethylene glycol. Chlorite is characterized by the first-order peak at 14 Å and a third-order peak at 4.7 Å which do not expand when glycolated. After heating to 550ºC, the 14 Å reflection is enhanced and shifts its position to 13.8 Å. Some Al-rich chlorite was observed in samples where the peak at 4.7 Å did not disappear totally after HCl treatment (Fe-Mg-rich chlorite was dissolved).

The illite chemistry index and illite crystallinity were calculated from the XRD patterns. The illite chemistry index refers to the ratio of the 5 Å and 10 Å peak areas (Esquevin, 1969). Ratios for the illite chemistry index of <0.5 represent Fe-Mg-rich illites; ratios >0.5 are found in Al-rich illites (Esquevin, 1969). Illite crystallinity was determined by measuring the full width at half maximum height (FWHM) of the 10 Å peak. Smaller values of illite crystallinity represent greater crystallinity and the numerical value increases with decreasing crystallinity (Kübler, 1967).

Goethite and hematite were identified by diffuse reflectance spectroscopy (DRS). Goethite was also identified by thermal treatment following Zhou *et al.* (2010) in which samples were heat treated in a muffle furnace for 2 h at 300ºC and solubilized by a buffered sodium dithionite solution (pH = 4.8) for 2 h. Reflectance spectra of samples were analyzed in a Perkin-Elmer Lambda 900 spectrophotometer with a diffuse reflectance attachment (reflectance sphere) from 400 to 700 nm at room temperature. Ground samples were made into a slurry on a glass microslide with distilled water, smoothed, and dried slowly at low temperature (<40ºC) before spectral measurements.

Fe speciation extraction

Suspended matter was subjected to a three-stage extraction procedure commonly used to determine the availability of Fe for reaction with dissolved sulfide (Raiswell *et al.*, 1994; Poulton and Raiswell, 2002; Poulton and Canfield, 2005). Amorphous and crystalline Fe (oxyhydr)oxides (with the exception of magnetite) were solubilized by a buffered sodium dithionite solution (pH = 4.8) for 2 h. Replicate extractions indicate a precision of ± 3−4%. This Fe fraction is considered to be highly reactive (compared to other non-oxide or silicate minerals) and is termed Fe_{HR}. Poorly reactive Fe (Fe_{PR}), which is considered to be poorly reactive towards dissolved sulfide, was extracted in boiling 12 N HCl for 2 min (Berner, 1970; Raiswell *et al.*, 1994; Poulton and Raiswell, 2005). This technique extracts magnetite and partially attacks some layer silicate minerals, in addition to the minerals extracted by dithionite (thus $Fe_{PR} = Fe_{(HCl)} - Fe_{(dithionite)}$). Total Fe ($Fe_T$) was analyzed by XRF. The unreactive fraction ($Fe_U = Fe_T - Fe_{(HCl)}$) consists of residual silicate Fe. Fe_{HR} and Fe_{PR} measurements were done by inductively coupled plasma atomic emission spectroscopy (ICP-AES).

RESULTS AND DISCUSSION

SPM concentration and grain size

The monthly water discharge and suspended particulate matter concentration in the CR at Nanjing city during the second sampling period varied greatly with seasons (Figure 2, Table 1). During the sampling periods, water discharge varied between 10,400 m^3/s (January) and 44,200 m^3/s (July) at Datong Hydrographic station (a gauging station for the CR's total water and suspended sediment discharge in the river's lower reaches, ~150 km upstream from Nanjing). This volume is similar to the long-term average water discharge of the CR at Datong Hydrographic station (1962−1984), ~10,000 m^3/s in January and 50,000 m^3/s in July (Chen *et al.*, 2002). Most of the water discharge of the CR usually occurs during summer, with a peak average in July (Xu and Milliman, 2009). During the sampling period, the maximum monthly value occurred in July, 2007, during the flood season (data from http://www.hydrodata.gov.cn). The SPM concentration showed highly seasonal variations, ranging from 11.3 to 152 mg/L (Table 1) and was strongly related to discharge, with the maximum SPM concentration (152 mg/L) occurring in July, 2007. This is similar to the observations made in many other river systems, where SPM concentrations generally increase with increasing discharge (Milliman and Meade, 1983). The maximum monthly discharge occurs in July and is ~4 to 5 times that of the minimum in January, reflecting substantial water input from precipitation in the flood season.

Two typical samples of SPM were selected to investigate the difference in the grain-size distributions between the low water discharge period (December) and high water-discharge period (August) (Figure 3). The grain-size distributions of the two samples exhibited a stepwise decline in the fine fraction. The December sample exhibited a skewed distribution toward the finer end (Figure 3) relative to the August sample. The mean grain size value was 10.0 μm for August and 7.9 μm for December. The grain-size frequency distribution and mean grain-size value of the SPM showed that the grain size is controlled by the seasonal variation of water discharge, increasing with increasing discharge. The SPM fine fraction, on the other hand, increased during periods of low discharge.

Chemistry and mineralogy of SPM

The major-element compositions of the 13 SPM samples from the second year are expressed in terms of weight percentage (wt.%, Table 1). In order to examine the seasonal composition of the CR river particulates, major element abundances were normalized to the Upper

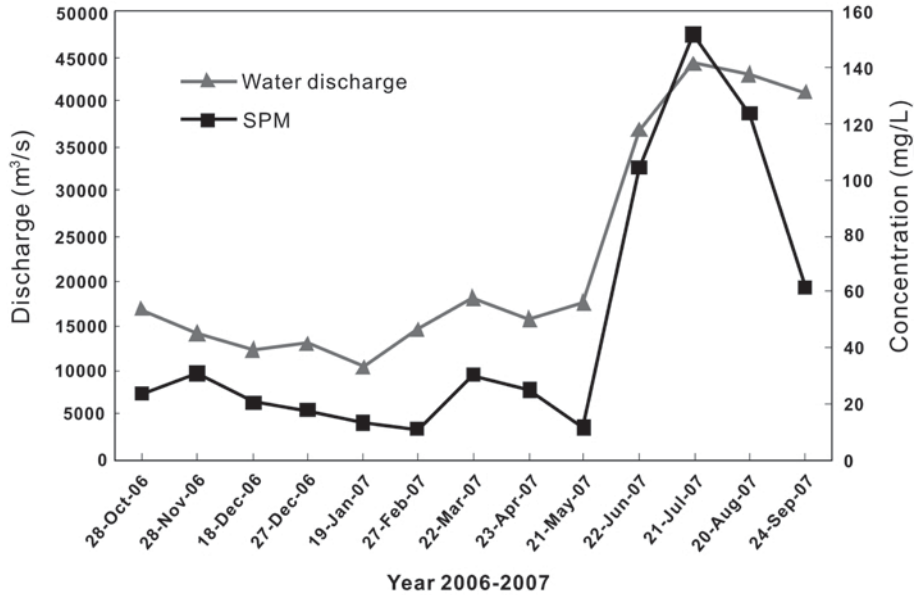

Figure 2. Monthly water discharge measured at the Datong Hydrographic Station during 2006–2007 and the monthly suspended particulate matter (SPM) concentrations.

Continental Crust (UCC) of Taylor and McLennan (1985), because sub-continental-scale rivers integrate the diversity of continental lithologies. Hence, the average parent-rock composition must be close to that of the average UCC (Gaillardet *et al.*, 1999a). Compared to the average UCC, the chemical elements can be classified into three groups (Figure 4). In the first group, Al_2O_3, Fe_2O_3, MnO, and TiO_2 showed positive anomalies during the hydrological cycle. These elements are known to be the least mobile during rock weathering. In the second group, SiO_2, Na_2O, and K_2O were depleted during the hydrological cycle. The depletion in Na_2O and K_2O is consistent with the relative mobility of these elements during weathering (Dupré *et al.*, 1996). Suspended loads are typically enriched in Al and depleted in Si compared to bedload (Galy and France-Lanord, 2001). Clays and primary micas were enriched in the suspended load, whereas quartz was more abundant in the coarse-grained fraction and tended to settle. Hence, the depletion in SiO_2 and enrichment in Al_2O_3 relative to the UCC were probably due to the sorting of the main minerals during transport and loss of large grain-sized quartz. In the last group, MgO and CaO were depleted relative to the UCC during low flow (dry

Table 1. Sampling details and chemical composition (wt.% oxide) based on XRF analysis of the SPM samples at the monitoring stations (Nanjing) for the second year.

Sample	Date	SPM (mg/L)	WT (ºC)[a]	Al_2O_3	CaO	Fe_2O_3	K_2O	MgO	MnO	Na_2O	P_2O_5	SiO_2	TiO_2	LOI	SUM
28-Oct-06	2006.10.28	23.8	no	19.23	2.73	7.40	2.99	2.19	0.13	0.58	0.23	50.95	0.91	12.18	99.51
28-Nov-06	2006.11.28	31.0	15	19.78	2.34	7.57	2.92	2.20	0.14	0.57	0.23	51.75	0.92	11.21	99.64
18-Dec-06	2006.12.18	20.8	9	19.88	1.79	7.40	3.03	1.90	0.13	0.58	0.21	53.47	0.88	10.54	99.82
27-Dec-06	2006.12.27	17.8	12	20.40	1.90	7.52	2.97	1.90	0.13	0.52	0.24	52.26	0.89	11.11	99.85
19-Jan-07	2007.01.19	13.1	14	19.62	1.99	7.31	3.02	1.96	0.15	0.53	0.23	52.41	0.86	11.38	99.47
27-Feb-07	2007.02.27	11.3	11	17.59	2.23	7.88	2.89	2.16	0.19	0.67	0.29	54.11	0.96	11.06	100.03
22-Mar-07	2007.03.22	30.1	10.5	18.78	1.91	7.40	2.93	2.04	0.15	0.60	0.23	54.51	0.92	10.14	99.61
23-Apr-07	2007.04.23	25.0	18	18.86	1.92	7.16	2.95	1.99	0.13	0.62	0.22	54.70	0.89	10.29	99.74
21-May-07	2007.05.21	12.0	23.2	21.01	1.11	7.32	3.07	1.85	0.10	0.44	0.24	51.96	0.78	11.71	99.60
22-Jun-07	2007.06.22	104.2	24.8	18.18	2.39	7.30	2.80	2.04	0.21	0.66	0.20	55.12	0.93	10.11	99.92
21-Jul-07	2007.07.21	152.0	26.5	15.47	4.26	6.96	2.75	2.65	0.15	0.90	0.19	55.16	0.96	10.03	99.48
20-Aug-07	2007.08.20	124.0	29.6	15.84	4.88	7.21	2.94	2.95	0.15	0.82	0.20	52.59	0.97	10.86	99.42
24-Sep-07	2007.09.24	61.8	27.5	16.69	4.36	7.18	3.07	2.87	0.14	0.84	0.20	52.97	0.93	10.48	99.73
UCC (upper crust)[b]				15.20	4.20	5.00	3.40	2.20	0.08	3.90	0.16	66.0	0.50		

[a] Water temperature; no = not observed
[b] Upper Continental Crust; data from Taylor and McLennan (1985).

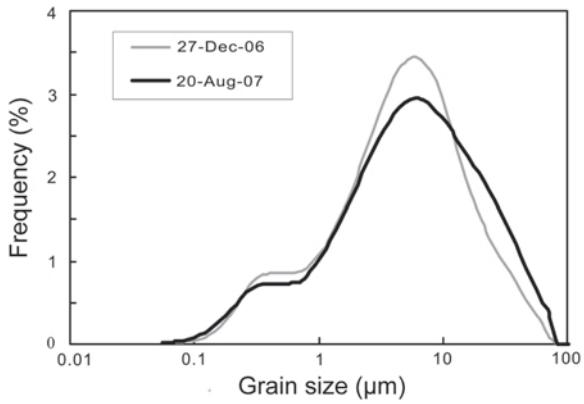

Figure 3. Grain size distributions of two typical samples selected from the SPM samples. The lighter-colored line is the dry season sample (27 Dec 2006) whereas the darker line is the flood season sample (20 Aug 2007).

seasons), but were enriched and showed positive anomalies during high-flow periods (flood season). Larger seasonal fluctuations were observed for CaO, MgO, Na_2O, and Al_2O_3. CaO, MgO, and Na_2O concentrations increased with increasing discharge and, therefore, exhibited their maximum concentration in the summer. Al_2O_3 showed the opposite seasonal pattern, which decreased sharply with increasing discharge.

The XRD patterns of bulk SPM samples showed that the main mineral phases in the suspended matter are quartz, plagioclase, K-feldspar, dolomite, calcite, and clay minerals (Figure 5). Semi-quantitative XRD analyses indicated that quartz (mean 21.8%) and clay minerals (mean 58.1%, except chlorite) are the major minerals in the bulk samples (Table 2). Plagioclase (mean 10%), K-feldspar (mean 2.5%), dolomite (mean 4%), and calcite (mean 3.6%) are minor components. Dolomite, calcite, and plagioclase showed striking seasonal variations and increased with increasing discharge; the maximum concentration of these minerals was during the flood season (summer) (Figure 5). In contrast, the clay-mineral content exhibited the opposite trend with the smallest concentrations in the flood season. Quartz did not change significantly with season and remained roughly constant between 19.4 and 25.3 wt.%.

The seasonal variations in terms of the minerals probably account for the chemical changes noted above also. A strong correlation (Figure 6) was found between chemical values and the main carriers of these minerals in the SPM. Calcite and dolomite are the main carriers of both CaO and MgO and they were more abundant in the SPM during flood season. Another distinctive feature of the major element distribution is the general increase of Na_2O and, hence, plagioclase (Na in SPM is primarily contained in feldspar, especially in plagioclase), during the flood season. The decrease in Al_2O_3 with increasing discharge appears related to the change in the abundance of the clay concentration which was at a minimum during the flood season (Figure 7).

The CR has a greater carbonate (calcite and dolomite) content (two or three-fold) in the flood-season SPM than during the dry season (Figure 7). The large increase in carbonate concentration in the summer is due to a greater physical denudation rate and stronger currents in the drainage areas. With the enhanced erosion rate during flood season, larger amounts of calcite and dolomite are brought to the river.

The total mass of Ca transported in dissolved form by rivers to the oceans was estimated to be 501 Mt/y (Berner and Berner, 1996). Of this, 326 Mt/y originates from carbonate dissolution (Gislason *et al.*, 2006) and the carbonate dissolution is also an important component in the global calcium cycle. Among the major rivers of the world, carbonate dissolution is particularly important

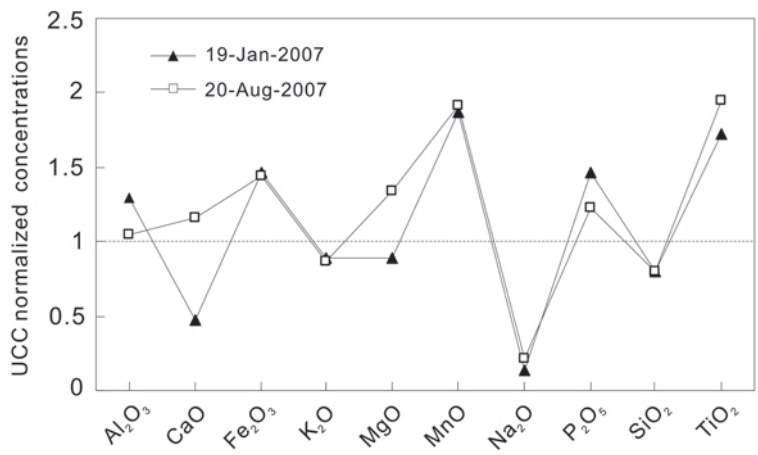

Figure 4. Upper Continental Crust (UCC) (Taylor and McLennan, 1985) normalized diagrams of two typical samples selected from the set of SPM samples (Nanjing). The dry season sample was taken on 19 Jan 2007 and the flood season sample on 20 Aug 2007. The strong seasonal change in CaO and MgO is indicated.

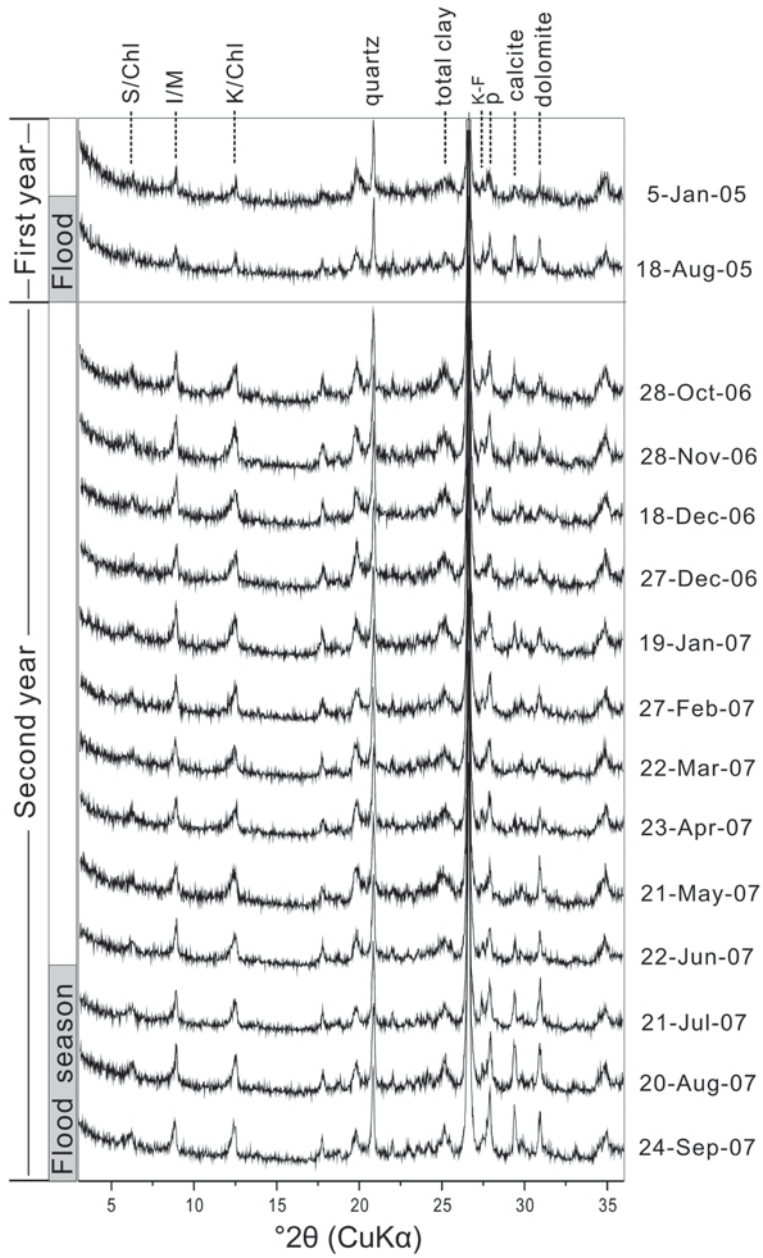

Figure 5. XRD patterns of the SPM samples (Nanjing). Abbreviations: K-F = K-feldspar, p = plagioclase, S/Chl = smectite/chlorite, I/M = illite/mica, K/Chl = kaolinite/chlorite.

for the CR in which >50% of the total dissolved solids (TDS) originates from carbonate weathering (Gaillardet *et al.*, 1999b). This large amount of dissolved carbonate is attributed to the widespread abundance of carbonate rocks in the CR drainage basin, particularly in the southern part and upper reaches. Carbonate weathering dominates river chemistry (Chen *et al.*, 2002). Those authors also reported that the concentrations of Ca^{2+}, Mg^{2+}, and HCO_3^- of the CR water do not show great seasonal variations over the period of 1 y, though they are slightly smaller in the summer high-flow period due to the large water discharge. The 4- to 5-fold increase in water discharge in the flood season would be expected to greatly dilute these major ion concentrations. One possible source of these ions is the enhanced dissolution of carbonate rocks in the basin during the flood season (Chen *et al.*, 2002). Carbonate weathering has a greater sensitivity to runoff because of the greater dissolution rates of carbonate relative to silicate (Tipper *et al.*, 2006). Szramek *et al.* (2007) observed that calcite and

Table 2. Mineralogical composition (%) of the SPM.

Sample	Quartz	Calcite	Dolomite	Plagioclase	K-feldspars	Clay
D (Å)	4.26	3.03	2.87-2.90	3.18-3.19	3.21-3.23	4.4
CF[a]	100/35	1.65	1.53	2.8	2	20[b]
5-Jan-05	19.5	7.5	5.8	11.3	3.1	52.8
18-Aug-05	20.3	1.9	1.6	6.9	1.6	67.7
28-Oct-06	20.0	3.9	3.1	10.2	2.7	60.1
28-Nov-06	21.1	3.1	3.5	10.2	3.1	59.0
18-Dec-06	24.0	1.8	2.2	8.8	1.4	61.7
27-Dec-06	19.4	2.4	2.4	6.3	1.2	68.2
19-Jan-07	20.7	4.1	3.3	9.2	3.9	58.7
27-Feb-07	25.3	2.1	4.2	11.5	2.3	54.7
22-Mar-07	23.8	1.0	2.7	9.5	0.0	63.0
23-Apr-07	22.1	1.9	3.0	9.1	4.1	59.9
21-May-07	20.4	1.4	5.6	7.7	1.3	63.7
22-Jun-07	25.2	3.2	4.7	9.3	2.0	55.6
21-Jul-07	23.5	6.0	6.9	12.2	5.5	45.8
20-Aug-07	20.6	6.7	5.8	12.6	2.3	52.0
24-Sep-07	21.7	7.0	6.0	14.8	2.4	48.1

[a] Correction Factors: Cook *et al*. (1975)
[b] Total clay minerals (except chlorite): Boski *et al*. (1998)

dolomite dissolution kept pace with increasing river discharge in two low-elevation humid temperate watersheds, and indicated that carbonate weathering is limited only by water flux and solubilities. The intrinsically greater dissolution rate of carbonates and their greater abundance in the SPM during the flood season would increase dissolution of detrital calcite and dolomite in river water. Thus, the present study suggests that carbonate rocks of the CR basin not only have been strongly weathered chemically, but also exhibit strong physical weathering during the flood season.

Clay mineral composition

Based on XRD analyses (Figure 8), the clay mineral assemblages in suspended particles of the CR included kaolinite, illite, smectite, and chlorite. The most abundant clay minerals in suspended particles was illite (44−62%), followed by kaolinite (12−39%) and chlorite (16−24%) (Figure 9). The illite concentration was similar to the average illite content of world rivers, which is between 45% and 60% (Irion, 1991). Smectite in the clay fractions was usually <5%, varying from trace to ~5% with an average of ~2%. The clay mineral distribution of the SPM from the CR was similar to that of other Himalayan rivers (the Ganges, Brahmaputra, Gandak, and Yamuna), which are characterized by the presence of large amounts of illite, equal amounts of kaolinite and chlorite, and little or no mixed-layer clays or smectite (Jha *et al.*, 1993).

Clay minerals in the suspended samples showed a distinct seasonal variation (Figure 9). Illite was at its most concentrated during the flood season (July–September) and at its least concentrated during the dry season (December−January), 60−66% and 44−45%, respectively. On the contrary, kaolinite had the smallest concentration in summer and the greatest concentration in winter, 12−15% and 32−36%, respectively. Compared to illite and kaolinite, the concentrations of smectite and chlorite displayed less seasonal variation during the sampling year.

The illite chemistry index of the SPM varied between 0.45 and 1.01, with a minimum value in flood season, and illite crystallinity varied between 0.55 and 0.85 ($^{o}\Delta 2\theta$), also with a minimum value in flood season. Illites in the CR SPM are considered to be of detrital origin, derived from soils, sediments, and rocks in the river watershed, and thus the crystallinity and chemistry index of illites are largely determined by provenance. Generally, a large illite crystallinity value in the sediments indicates highly degraded illites, whereas small values indicate relatively unaltered illites (Chamley, 1989; Ji *et al.*, 1999). Fe-Mg-rich illites are more susceptible to weathering than Al-rich members. Larger values in both the chemistry index and crystallinity of illites in the SPM may indicate a greater input of weathered illites, and *vice versa*.

Correlation of the kaolinite/illite ratio with the illite chemistry index and illite crystallinity (Figure 10) revealed that these three mineralogical parameters from flood season were much lower than those of the low-flow seasons. Increases in the illite chemistry index and illite crystallinity values are associated with increased kaolinite/illite ratios. These results suggest that a strengthened physical erosion of source rocks in the basin during flood seasons results in an increased contribution of the proportion of less weathered illite to the river system. This is mainly due to the influence of the Asian monsoon system which causes greater

precipitation in the flood season. Variations in clay mineral assemblages of the SPM are, therefore, controlled mainly by changes in erosion and transport patterns.

The species and proportions of individual clay minerals in soils and sediments depend mainly on the climatic conditions and on the nature of the source rocks. Clay minerals can be advected over long distances and settle far away from their source area so they are utilized as indicators of environmental change and pathways of suspended sediment distribution (Chamley, 1989; Weaver, 1989).

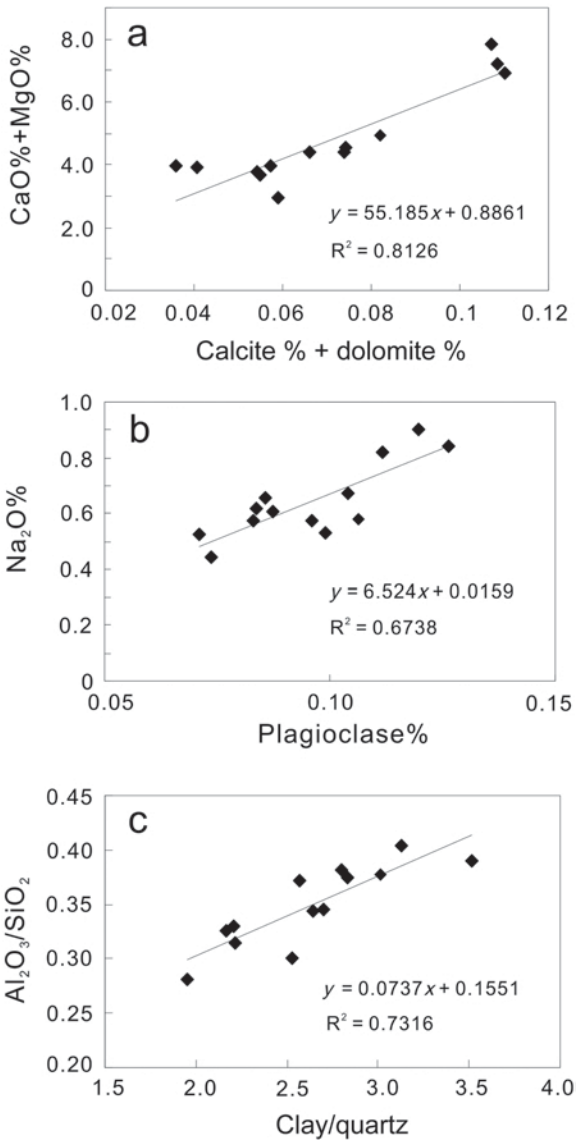

Figure 6. Correlations between chemical data and mineral content: (a) CaO%+MgO% *vs*. calcite% + dolomite%, (b) Na_2O% *vs*. plagioclase%, (c) Al_2O_3/SiO_2 *vs*. clay/quartz. Note that the chemical data and mineral content show good correlation in the SPM.

The CR sediment comes mainly from the NW of the CR basin, because this area contains more erodible soils and steep mountains (Xu *et al.*, 2007). The upper CR basin plays an important role in this process because it supplies most of the suspended sediments to the ocean (Yang *et al.*, 2002; Chen *et al.*, 2008). The collision of India and Asia resulted in the buildup of the Himalayas and the Tibetan Plateau where incident solar heating in the summer drives strong atmospheric convection and rainfall associated with the Asian monsoon (Raymo and Ruddiman, 1992). The Upper CR drains the East Tibetan Plateau, and flow volume is controlled by a monsoon climate in which precipitation and runoff change seasonally. About 70% of the annual precipitation falls during the summer (June, July, and August) and ~50% of the annual water discharge occurs from July to September. Hence, most of the physical erosion takes place during the summer and sediment discharge is highly concentrated from July to September (Lu *et al.* 2003). The plateau zone allows physical weathering processes and forms lithosols containing illite and chlorite (Liu *et al.*, 2003).

The relative increase in illite concentration can be related to an increase in the mechanical erosion rate in

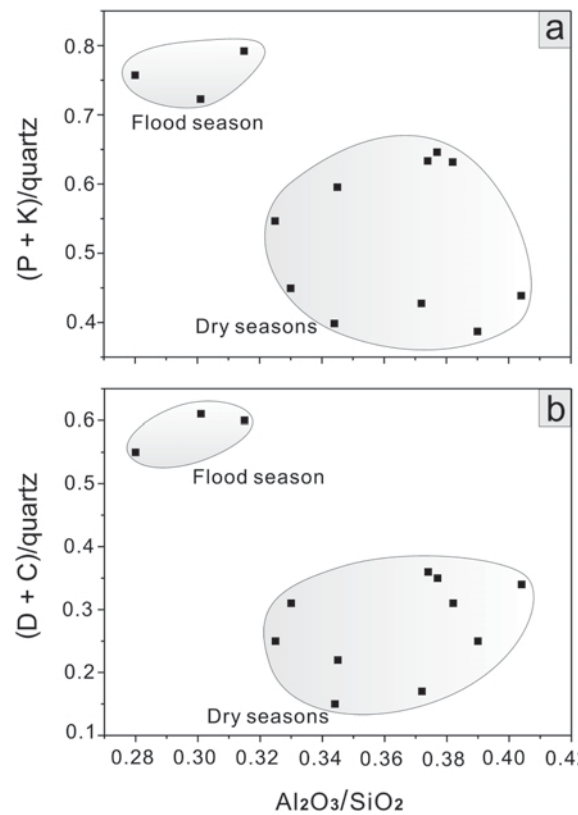

Figure 7. Correlations of the Al_2O_3/SiO_2 ratio with (a) (plagioclase + K-feldspar)/quartz ratio and (b) (dolomite + calcite)/quartz ratio for SPM (second year).

this region (the upper basin) during the flood season. The upper basin runs mainly through the Qinghai-Tibet Plateau and has a number of major tributaries, where the exposed rocks are clastic sedimentary (including Jurassic red sandstone), igneous, and metamorphic. These rocks contain abundant micaceous minerals that easily produce abundant illites by physical erosion and limited chemical weathering. The relatively good agreement in the three mineralogical parameters between the flood-season samples taken at Nanjing (lower reaches) and Chongqing (upper reaches) suggests that the upper basin of the CR is an important source of illite during the flood season (Figure 10).

In contrast, during the dry season, physical erosion of the upper basin becomes weaker. The large illite chemistry index and illite crystallinity values associated with the kaolinite/illite ratio during the dry season is interpreted to reflect a decreasing supply of well crystallized illite delivered from the upper drainage basin and increasing proportions of poorly crystallized illite and kaolinite input from middle–lower reaches of the CR to the suspended load. In the middle and lower reaches of the river, Quaternary fluvial and lacustrine sediments are common and provide more mature material. Furthermore, channel erosion of the lower reaches was enhanced after dam construction, thereby increasing the relative contribution of more weathered clay minerals to the suspended load in dry seasons (Chen *et al.*, 2001; Xu and Milliman, 2009).

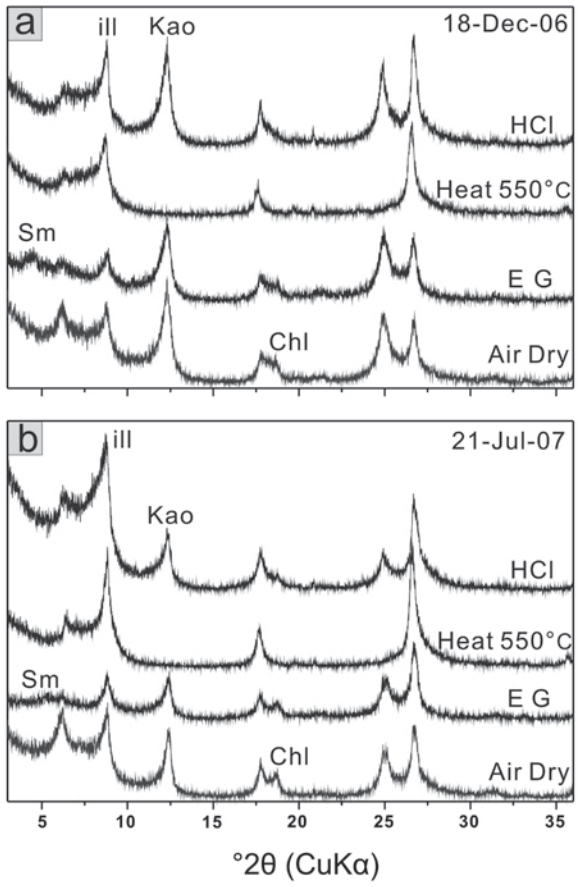

Figure 8. XRD patterns of selected samples of SPM: (a) dry season (18 Dec 2006) and (b) flood season (21 Jul 2007). The samples were analyzed untreated (Air Dry), ethylene glycol-solvated (EG), heated at 550ºC (heated 550ºC), and HCl treated (HCl). Abbreviations: ill = illite, Kao = kaolinite, Sm = smectite, Chl = chlorite.

Speciation and mineralogy of iron in SPM

Iron concentration and speciation, as well as mineral phases of the SPM (2006–2007, Nanjing), were examined to investigate Fe reactivity. A method of selective sequential dissolution was employed that distinguished between three operationally defined Fe fractions: highly reactive iron (Fe_{HR}), poorly reactive iron (Fe_{PR}), and unreactive iron (Fe_U) (Poulton and Raiswell, 2002). The total Fe content ranged from 4.87 to 5.52% and displayed a slight seasonal variation with water discharge. Total Fe has the lowest concentration during the high-flow period. The Fe_{HR} content of the SPM ranges from 1.91 to 2.62% with a mean of 2.3%. The Fe_{HR} exhibited a similar seasonal variability to that of the total Fe with the smallest values (1.91%) observed in July (Table 3 and Figure 11). The values of Fe_{HR} in flood season were similar to previous observations by Poulton and Raiswell (2002).

The slight seasonal changes in Fe_T and Fe_{HR} in SPM were probably a result of "hydrodynamic sorting" whereby finer particles, which are generally enriched in Fe, especially Fe_{HR} (Poulton and Raiswell, 2005), were preferentially transported during the low-flow period, while coarser particles were delivered during the summer flood due to the larger erosion and carrying capacity. Fe_{HR}/Fe_T of the SPM of the CR ranged from 0.39 to 0.51 with a mean of 0.45, very close to the global mean riverine SPM value (Fe_{HR}/Fe_T = 0.43, Poulton and Raiswell, 2002). The smallest Fe_{HR}/Fe_T value was 0.39, observed in July and August, and nearly identical to the previously reported level of 0.38 in July, 1997 (Poulton and Raiswell, 2002).

The mineralogical interpretation of Fe_{HR} was explored using DRS, which is especially sensitive to Fe (oxyhydr)oxides in soils and sediments, and has been used as an ancillary method to identify and estimate Fe oxides in soils and sediments (Deaton and Balsam, 1991; Ji *et al.*, 2002; Balsam and Beeson, 2003). First derivative value (FDV) curves of the visible DRS patterns are excellent qualitative indicators and potentially useful for quantitatively determining hematite concentration (Barranco *et al.*, 1989). The primary VIS first-derivative peak for goethite is at 535 nm with a secondary peak at 435 nm. A single prominent peak between 565 and 585 nm is associated with hematite. The FDV curves of the SPM of CR (Figure 12) showed

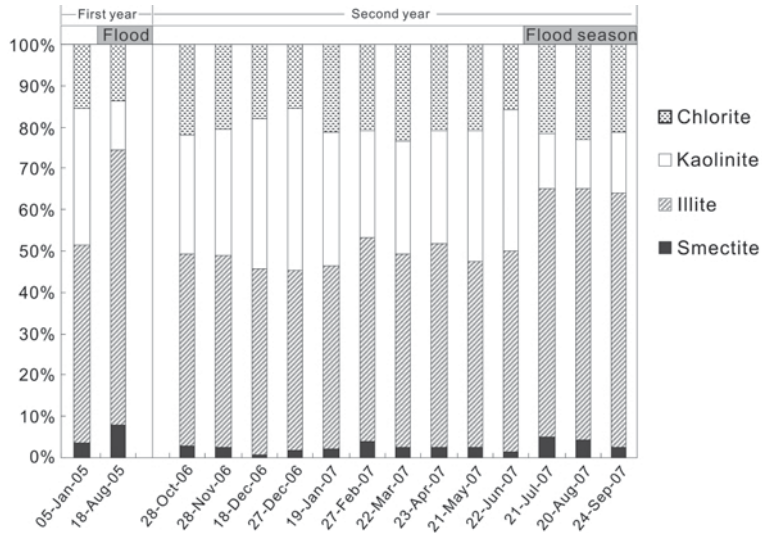

Figure 9. Seasonal changes for the clay mineral composition of the SPM (Nanjing).

two diagnostic peaks, a small sharp peak at 435 nm, and a major, wide peak between 505 and 585 nm. The first peak was attributed to the secondary FDV peak of the goethite, and the latter to the superposition of the primary peaks of goethite and hematite. These DRS signals disappeared after the dithionite treatment (Figure 12), indicating unambiguously that goethite and hematite account for the main Fe mineral phases in Fe_{HR}. The DRS patterns of the SPM from CR showed a significant shift of the FDV peak toward longer wavelengths after thermal treatment at 300ºC for 2 h (Figure 12) as a result of goethite dehydration (Zhou *et al.*, 2010), suggesting that, of Fe_{HR}, goethite is the dominant Fe mineral. Furthermore, the wavelength position of the FDV peak maximum of the mixture depended mainly on the concentration of hematite (Barranco *et al.*, 1989; Zhou *et al.*, 2010). The primary FDV peak wavelength was ~565 nm when the hematite content was <0.4%, and it moved to 575 nm when the hematite content exceeded 0.4%. The FDV curves of the SPM samples displayed a maximum FDV at ~565 nm, suggesting that hematite is <0.4% and goethite is probably the dominant Fe mineral in the SPM studied.

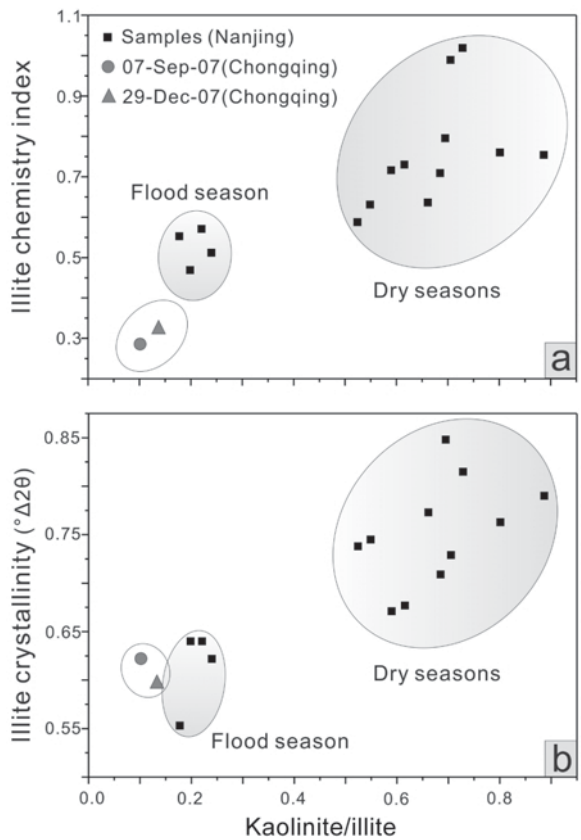

Figure 10. Correlations of kaolinite/illite ratio with (a) illite chemistry index and (b) illite crystallinity for SPM. For reference, samples from upper reaches of the CR taken at Chongqing city are plotted as gray dots (7 Sep 2007) and gray triangles (29 Dec 2007), respectively.

The rates of sediment delivery to ocean basins by rivers are difficult to quantify, in part because temporal variability of clastic fluxes requires frequent sampling over prolonged intervals (Raiswell *et al.*, 2006). In addition, human activities, such as dam construction, have significantly modified the patterns of water and sediment delivery. Recent studies show that the suspended sediment load of the CR was substantially decreased after the TGD (Figure 1) came on line in 2004 (Xu *et al.*, 2006). Based on monthly data, the calculated Fe_T flux and Fe_{HR} flux are 2.78×10^6 T/y and 1.19×10^6 T/y, respectively. High-flow season (June to September) contributes ~87% of the annual Fe_T and Fe_{HR} loads. Data generated by the current study will provide a new and more precise estimate of the

Table 3. Iron speciation characteristics for the SPM (second year).

Sample	Fe_{HR} (%)	Fe_H (%)	FeT (%)	Al_T (%)	Fe_U	Fe_{PR}	Fe_{HR}/FeT	Fe_{PR}/FeT	Fe_U/FeT	Fe_T/Al_T
28-Oct-06	2.37	3.31	5.18	10.18	1.87	0.93	0.46	0.18	0.36	0.51
28-Nov-06	2.47	3.38	5.30	10.47	1.93	0.90	0.47	0.17	0.36	0.51
18-Dec-06	2.37	3.27	5.18	10.53	1.91	0.90	0.46	0.17	0.37	0.49
27-Dec-06	2.51	3.37	5.26	10.80	1.89	0.86	0.48	0.16	0.36	0.49
19-Jan-07	2.39	3.37	5.12	10.39	1.75	0.98	0.47	0.19	0.34	0.49
27-Feb-07	2.43	3.67	5.52	9.31	1.84	1.24	0.44	0.22	0.33	0.59
22-Mar-07	2.20	3.15	5.18	9.94	2.04	0.95	0.42	0.18	0.39	0.52
23-Apr-07	2.13	3.14	5.02	9.98	1.88	1.01	0.42	0.20	0.37	0.50
21-May-07	2.32	3.15	5.13	11.12	1.97	0.83	0.45	0.16	0.38	0.46
22-Jun-07	2.62	3.01	5.11	9.63	2.09	0.39	0.51	0.08	0.41	0.53
21-Jul-07	1.91	3.01	4.87	8.19	1.86	1.10	0.39	0.23	0.38	0.60
20-Aug-07	1.98	3.10	5.05	8.39	1.95	1.12	0.39	0.22	0.39	0.60
24-Sep-07	2.23	3.04	5.02	8.83	1.98	0.81	0.44	0.16	0.39	0.57
Mean	2.30	3.23	5.15	9.83	1.92	0.93	0.45	0.18	0.37	0.52
Jul-1997[a]	1.86	3.58	4.92		1.34	1.72	0.38	0.35	0.27	

[a] Poulton and Raiswell (2002)

suspended particulate Fe fluxes supplied by the CR to the Pacific Ocean, especially after impoundment of the Three Gorges Dam.

CONCLUSIONS

(1) The concentration of CR SPM ranged from 11.3 to 152 mg/L and is correlated to the rate of water discharge. The SPM had a greater concentration of coarse-fraction material during the flood season with a larger water discharge than during the dry season with less water discharge.

(2) Most major elements and minerals of CR SPM exhibited a seasonal change in their abundances. Larger seasonal fluctuations were observed for CaO, MgO, Na_2O, and Al_2O_3. CaO, MgO, and Na_2O increased with increasing discharge, whereas Al_2O_3 decreased sharply with increasing discharge. Dolomite, calcite, and plagioclase showed similar striking seasonal variations, and increased with increasing discharge, having their maximum concentrations during the flood season. In contrast, the clay-mineral content followed the opposite trend, with the smallest concentrations during the flood season.

(3) The large increase in carbonate concentration during the summer could reflect enhanced physical erosion of carbonate rocks in the upper CR basin during flood season. Carbonate rocks of the CR basin have suffered both strong chemical and physical weathering during the summer.

(4) Illite dominated the clay minerals of CR SPM, followed by chlorite, kaolinite, and smectite. The abundances of illite and kaolinite showed distinctly seasonal variations. The SPM had more illite and less

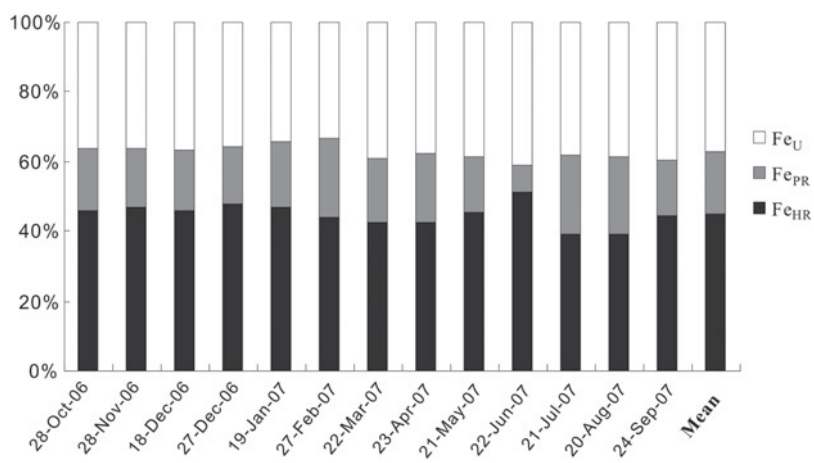

Figure 11. Relative proportions of Fe_{HR}, Fe_{PR}, and Fe_U in SPM (Nanjing) during 2006–2007.

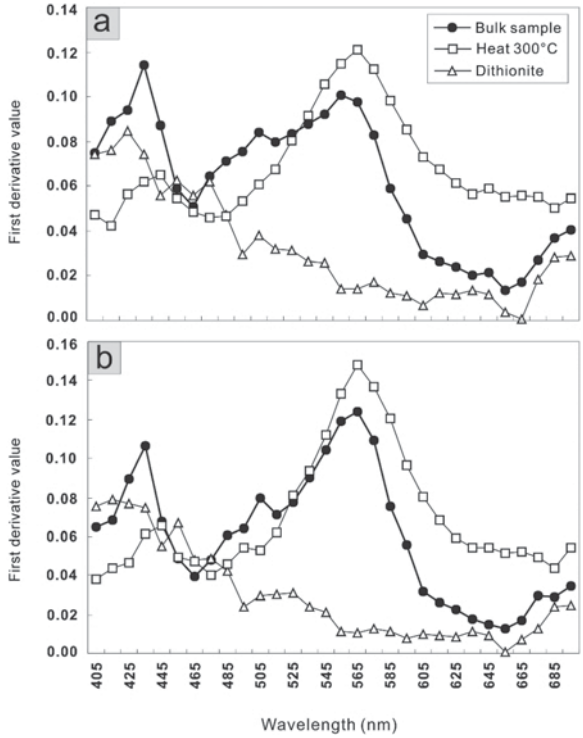

Figure 12. First derivative (FDV) curves in the visible region of two representative SPM samples: (a) dry season sample (19 Jan 2007), (b) flood season sample (20 Aug 2007). FDV curves show two diagnostic DRS peaks, goethite at 435 nm and a mixture of goethite with minor hematite between 505 nm and 565 nm. The DRS signals disappeared after dithionite treatment (triangle line), demonstrating that goethite and hematite are major mineral phases of the Fe_{HR} fraction.

kaolinite during the flood season than during the dry season. The illite chemistry index and crystallinity, as well as kaolinite/illite ratio, all indicated intense physical erosion of CR during the rainy season.

(5) The total Fe (Fe_T) and highly reactive Fe (Fe_{HR}) concentrations displayed similar seasonal changes with the smallest values observed during the flood season. Goethite was the dominant Fe (oxyhydr)oxide mineral phase of the CR SPM and hematite was a minor component, as revealed by DRS analyses. The Fe_T flux and Fe_{HR} flux are currently 2.78×10^6 T/y and 1.19×10^6 T/y, respectively, after impoundment at the TGD, which caused a sharp reduction in the sediment load of the CR.

ACKNOWLEDGMENTS

The present research was funded by the National Basic Research Program of China (2004CB720204) and the National Natural Science Foundation of China (Grants No. 40625012 and 40830107). The authors thank Associate Editor, Ray E. Ferrell, and reviewer John S. Compton for their thoughtful comments which significantly improved the manuscript.

REFERENCES

Balsam, W.L. and Beeson, J.P. (2003) Sea-floor sediment distribution in the Gulf of Mexico. *Deep-Sea Research Part I*, **50**, 1421–1444.

Barranco, F.T., Balsam, W.L., and Deaton, B.C. (1989) Quantitative reassessment of brick red lutites: Evidence from reflectance spectrophotometry. *Marine Geology*, **89**, 299–314.

Berner, R.A. (1970) Sedimentary Pyrite Formation. *American Journal of Science*, **268**, 1–23.

Berner, E.K. and Berner, R.A. (1996) *Global Environment: Water, Air, and Geochemical Cycles*. Prentice Hall, Englewood Clifts, New Jersey, USA, 376 pp.

Biscaye, P.E. (1965) Mineralogy and sedimentation of recent deep-sea clay in the Atlantic Ocean and adjacent seas and oceans. *Geological Society of America Bulletin*, **76**, 803–832.

Borch, T., Masue, Y., Kukkadapu, R.K., and Fendorf, S. (2007) Phosphate imposed limitations on biological reduction and alteration of ferrihydrite. *Environmental Science Technology*, **41**, 166–172.

Boski, T., Pessoa, J., Pedro, P., Thorez, J., Dias, J.M.A., and Hall, I.R. (1998) Factors governing abundance of hydrolysable amino acids in the sediments from the NW European Continental margin (47–50ºN). *Progress in Oceanography*, **42**, 145–164.

Chamley, H. (1989) *Clay Sedimentology*. Springer-Verlag, Berlin.

Chen, J.S., Wang, F.Y., Xia, X.H., and Zhang, L.T. (2002) Major element chemistry of the Changjiang (Yangtze River). *Chemical Geology*, **187**, 231–255.

Chen, X.Q., Yan, Y.X., Fu, R.S., Dou, X.P., and Zhang, E.F. (2008) Sediment transport from the Yangtze River, China, into the sea over the Post-Three Gorge Dam Period: A discussion. *Quaternary International*, **186**, 55–64.

Chen, Z.Y., Li, J.F., Shen, H.T., and Wang, Z.H. (2001) Yangtze River of China: Historical analysis of discharge variability and sediment flux. *Geomorphology*, **41**, 77–91.

Chetelat, B., Liu, C., Zhao, Z., Wang, Q., Li, S., Li, J., and Wang, B. (2008) Geochemistry of the dissolved load of the Changjiang Basin rivers: anthropogenic impacts and chemical weathering. *Geochimica et Cosmochimica Acta*, **72**, 4254–4277.

Cook, H.E., Johnson, P.D., Matti, J.C., and Zemmels, I. (1975) Methods of sample preparation and x-ray diffraction analysis in x-ray mineralogy laboratory. Pp. 997–1007 in: *Initial Reports of the DSDP* (A.G. Kaneps *et al.*, editors). Printing Office, Washington, D.C.

Cornell, R.M. and Schwertmann, U. (2003) *The Iron Oxides: Structure, Properties, Reactions, Occurrence and Uses*. VHC, New York.

Deaton, B.C. and Balsam, W.L. (1991) Visible spectroscopy – a rapid method for determining hematite and goethite concentration in geological materials. *Journal of Sedimentary Petrology*, **61**, 628–632.

Dekov, V.M., Komy, Z., Araujo, F., VanPut, A., and VanGrieken, R. (1997) Chemical composition of sediments, suspended matter, river water and ground water of the Nile (Aswan-Sohag traverse). *Science of the Total Environment*, **201**, 195–210.

Ding, T., Wan, D., Wang, C., and Zhang, F. (2004) Silicon isotope compositions of dissolved silicon and suspended matter in the Yangtze River, China. *Geochimica et Cosmochimica Acta*, **68**, 205–216.

Duan, S.W., Liang, T., Zhang, S., Wang, L.J., Zhang, X.M., and Chen, X.B. (2008) Seasonal changes in nitrogen and phosphorus transport in the lower Changjiang River before the construction of the Three Gorges Dam. *Estuarine*

Coastal and Shelf Science, **79**, 239–250.

Dupré, B., Gaillardet, J., Rousseau, D., and Allegre, C.J. (1996) Major and trace elements of river-borne material: the Congo basin. *Geochimica et Cosmochimica Acta*, **60**, 1301–1321.

Eberl, D.D. (2004) Quantitative mineralogy of the Yukon River system: Changes with reach and season, and determining sediment provenance. *American Mineralogist*, **89**, 1784–1794.

Esquevin, J. (1969) *Influence de la composition chimique des illites sur le cristallinité*. Bulletin Centre Recherch Pau, S.N.P.A, **3**, 147–154.

Fung, I.Y., Meyn, S.K., Tegen, I., Doney, S.C., John, J.G., and Bishop, J.K.B. (2000) Iron supply and demand in the upper ocean. *Global Biogeochemical Cycles*, **14**, 281–296.

Gaillardet, J., Dupre, B., and Allegre, C. J. (1999a) Geochemistry of large river suspended sediments: Silicate weathering or recycling tracer? *Geochimica et Cosmochimica Acta*, **63**, 4037–4051.

Gaillardet, J., Dupré, B., Louvat, P., and Allègre, C.J. (1999b) Global silicate weathering and CO_2 consumption rates deduced from the chemistry of large rivers. *Chemical Geology*, **159**, 3–30.

Galy, A. and France-Lanord, C. (2001) Higher erosion rates in the Himalaya: Geochemical constraints on riverine fluxes. *Geology*, **29**, 23–26.

Gao, S. and Wang, Y.P. (2008) Changes in material fluxes from the Changjiang River and their implications on the adjoining continental shelf ecosystem. *Continental Shelf Research*, **28**, 1490–1500.

Gimsing, A.L. and Borggaard, O.K. (2007) Phosphate and glyphosate adsorption by hematite and ferrihydrite and comparison with other variable-charge minerals. *Clays and Clay Minerals*, **55**, 108–114.

Gingele, F.X., De Deckker, P., and Hillenbrand, C.D. (2001) Clay mineral distribution in surface sediments between Indonesia and NW Australia – source and transport by ocean currents. *Marine Geology*, **179**, 135–146.

Gislason, S.R., Oelkers, E.H., and Snorrason, A. (2006) Role of river-suspended material in the global carbon cycle. *Geology*, **34**, 49–52.

Guyot, J.L., Jouanneau, J.M., Soares, L., Boaventura, G.R., Maillet, N., and Lagane, C. (2007) Clay mineral composition of river sediments in the Amazon Basin. *Catena*, **71**, 340–356.

Haese, R.R. (2006) The biogeochemistry of iron. Pp. 241–270 in: *Marine Geochemistry* (H.D. Schulz and M. Zabel, editors). 2nd edition. Springer-Verlag Heidelberg, New York.

Hu, M.H., Stallard, R.F., and Edmond, J.M. (1982) Major ion chemistry of some large Chinese rivers. *Nature*, **298**, 550–553.

Irion, G. (1991) Minerals in rivers. Pp. 265–281 in: *Biogeochemistry of Major World Rivers* (E.T. Degens, S. Kempe, and J.F. Richey, editors). SCOPE, **42**. Wiley, New York.

Jha, P.K., Vaithiyanathan, P., and Subramanian, V. (1993) Mineralogical characteristics of the sediments of a Himalayan river: Yamuna river – a tributary of the Ganges. *Environmental Geology*, **22**, 13–20.

Ji, J.F., Chen, J., and Lu, H.Y. (1999) Origin of illite in the loess from the Luochuan area, Loess Plateau, Central China. *Clay Minerals*, **34**, 525–532.

Ji, J.F., Balsam, W., Chen, J., and Liu, L.W. (2002) Rapid and quantitative measurement of hematite and goethite in the Chinese loess-paleosol sequence by diffuse reflectance spectroscopy. *Clays and Clay Minerals*, **50**, 208–216.

Jickells, T.D., An, Z.S., Andersen, K.K., Baker, A.R., Bergametti, G., Brooks, N., Cao, J.J., Boyd, P.W., Duce, R.A., Hunter, K.A., Kawahata, H., Kubilay, N., LaRoche, J., Liss, P.S., Mahowald, N., Prospero, J.M., Ridgwell, A.J., Tegen, I., and Torres, R. (2005) Global iron connections between desert dust, ocean biogeochemistry, and climate. *Science*, **308**, 67–71.

Kübler, B. (1967) La cristallinité de I' illite et les zones tout à fait supérieures du métamorphisme. Pp. 105–121 in: *Etages tectoniques, Colloque de Neuchâtel.* A La Bacconnière, Neuchâtel, Switzerland.

Koshikawa, M.K., Takamatsu, T., Takada, J., Zhu, M.Y., Xu, B.H., Chen, Z.Y., Murakami, S., Xu, K.Q., and Watanabe, M. (2007) Distributions of dissolved and particulate elements in the Yangtze estuary in 1997–2002: Background data before the closure of the Three Gorges Dam. *Estuarine Coastal and Shelf Science*, **71**, 26–36.

Li, Y.H., Teraoka, H., Young, T.S., and Chen, J.S. (1984) The elemental composition of suspended particles from the Yellow and Yangtze Rivers. *Geochimica et Cosmochimica Acta*, **48**, 1561–1564.

Liu, J.P., Xu, K.H., Li, A.C., Milliman, J.D., Velozzi, D.M., Xiao, S.B., and Yang, Z.S. (2007) Flux and fate of Yangtze river sediment delivered to the East China Sea. *Geomorphology*, **85**, 208–224.

Liu, Z.F., Trentesaux, A., Clemens, S.C., Colin, C., Wang, P.X., Huang, B.Q., and Boulay, S. (2003) Clay mineral assemblages in the northern South China Sea: implications for East Asian monsoon evolution over the past 2 million years. *Marine Geology*, **201**, 133–146.

Lu, X.X., Ashmore, P., and Wang, J.F. (2003) Seasonal water discharge and sediment load changes in the Upper Yangtze, China. *Mountain Research and Development*, **23**, 56–64.

Martin, J.M. and Meybeck, M. (1979) Elemental mass balance of material carried by major world rivers. *Marine Chemistry*, **7**, 173–206.

Milliman, J.D. and Meade, R.H. (1983) World-wide delivery of river sediment to the oceans. *Journal of Geology*, **91**, 1–21.

Muller, B., Berg, M., Yao, Z.P., Zhang, X.F., Wang, D., and Pfluger, A. (2008) How polluted is the Yangtze River? Water quality downstream from the Three Gorges Dam. *Science of the Total Environment*, **402**, 232–247.

Paige, C.R., Snodgrass, W.J., Nicholson, R.V., Scharer, J.M., and He, Q.H. (1997) The effect of phosphate on the transformation of ferrihydrite into crystalline products in alkaline media. *Water Air and Soil Pollution*, **97**, 397–412.

Petschick, R., Kuhn, G., and Gingele, F. (1996) Clay mineral distribution in surface sediments of the South Atlantic: sources, transport, and relation to oceanography. *Marine Geology*, **130**, 203–229.

Poulton, S.W. and Canfield, D.E. (2005) Development of a sequential extraction procedure for iron: implications for iron partitioning in continentally derived particulates. *Chemical Geology*, **214**, 209– 221.

Poulton, S.W. and Raiswell, R. (2002) The low temperature geochemical cycle of iron: from continental fluxes to marine sediment deposition. *American Journal of Science*, **302**, 774– 805.

Poutlon, S.W. and Raiswell, R. (2005) Chemical and physical characteristics of iron oxides in riverine and glacial meltwater sediments. *Chemical Geology*, **218**, 203–221.

Raiswell, R., Canfield, D.E., and Berner, R.A. (1994) A comparison of iron extraction methods for the determination of degree of pyritization and the recognition of iron-limited pyrite formation: *Chemical Geology*, **111**, 101–110.

Raymo, M.E. and Ruddiman, W.F. (1992) Tectonic forcing of late Cenozoic climate. *Nature*, **359**, 117–122.

Rovira, M., Gimenez, J., Martinez, M., Martinez-Llado, X., de Pablo, J., Marti, V., and Duro, L. (2008) Sorption of selenium(IV) and selenium(VI) onto natural iron oxides: Goethite and hematite. *Journal of Hazardous Materials*,

150, 279–284.

Szramek, K., McIntosh, J.C., Williams, E.L., Kanduc, T., Ogrinc, N., and Walthers, L.M. (2007) Relative weathering intensity of calcite versus dolomite in carbonate-bearing temperate zone watersheds: Carbonate geochemistry and fluxes from catchments within the St. Lawrence and Danube river basin. *Geochemistry Geophysics Geosystems*, **8**, Q04002.

Taylor, S.R. and McLennan, S.M. (1985) *The Continental Crust: its Composition and Evolution*. Blackwell, Oxford, London.

Thiry, M. (2000) Palaeoclimatic interpretation of clay minerals in marine deposits: an outlook from the continental origin. *Earth-Science Reviews*, **49**, 201–221.

Tipper, E.T., Bickle, M.J., Galy, A., West, A.J., Pomiés, C., and Chapman, H.J. (2006) The short term climatic sensitivity of carbonate and silicate weathering fluxes: insight from seasonal variations in river chemistry. *Geochimica et Cosmochimica Acta*, **70**, 2737–2754.

Viers, J., Dupre, B., and Gaillardet, J. (2009) Chemical composition of suspended sediments in World Rivers: New insights from a new database. *Science of the Total Environment*, **407**, 853–868.

Wang, Z.L., Zhang, J., and Liu, C.Q. (2007) Strontium isotopic compositions of dissolved and suspended loads from the main channel of the Yangtze River. *Chemosphere*, **69**, 1081–1088.

Weaver, C.E. (1989) *Clays, Muds and Shales*. Developments in Sedimentology, vol. **44**. Elsevier, Amsterdam, p. 819.

Xu, K.H. and Milliman, J.D. (2009) Seasonal variations of sediment discharge from the Yangtze River before and after impoundment of the Three Gorges Dam. *Geomorphology*, **104**, 276–283.

Xu, K.H., Milliman, J.D., Yang, Z.S., and Wang, H.J. (2006) Yangtze sediment decline partly from Three Gorges Dam. *Eos*, **87**, 185–190.

Xu, K.H., Milliman, J.D., Yang, Z.S., and Xu, H. (2007) Climatic and anthropogenic impacts on the water and sediment discharge from the Yangtze River (Changjiang), 1950–2005. Pp. 609–626 in: *Large Rivers: Geomorphology and Management* (A. Gupta, editor). John Wiley & Sons, West Sussex, England.

Xu, K.H., Milliman, J.D., Li, A.C., Liu, J.P., Kao, S.J., and Wan, S.M. (2009) Yangtze- and Taiwan-derived sediments on the inner shelf of East China Sea. *Continental Shelf Research*, **29**, 2240–2256.

Yang, S.L., Zhao, Q.Y., and Belkin, I.M. (2002) Temporal variation in the sediment load of the Yangtze river and the influences of human activities. *Journal of Hydrology*, **263**, 56–71.

Yang, S.Y., Jung, H.S., and Li, C.X. (2004) Two unique weathering regimes in the Changjiang and Huanghe drainage basins: geochemical evidence from river sediments. *Sedimentary Geology*, **164**, 19–34.

Zhang, C.S., Wang, L.J., Zhang, S., and Li, X.X. (1998) Geochemistry of rare earth elements in the mainstream of the Yangtze River, China. *Applied Geochemistry*, **13**, 451–462.

Zhang, J. (1999) Heavy metal compositions of suspended sediments in the Changjiang (Yangtze River) estuary: significance of riverine transport to the ocean. *Continental Shelf Research*, **19**, 1521–1543.

Zhang, J., Huang, W.W., Liu, M.G., and Zhou, Q. (1990) Drainage basin weathering and major element transport of two large Chinese rivers (Huanghe and Changjiang). *Journal of Geophysical Research – Oceans*, **95**, 13277–13288.

Zhou, W., Chen, L.X., Zhou, M., Balsam, W., and Ji, J.F. (2010) Thermal identification of goethite in soils and sediments by diffuse reflectance spectroscopy. *Geoderma*, **155**, 419–425.

(*Received 2 June 2009; revised 20 July 2010; Ms. 320; A.E. R.E. Ferrell*)